Characterization of a PET detector head based on continuous LYSO crystals and monolithic, 64-pixel silicon photomultiplier matrices.

G Llosá[1], J Barrio[1], C Lacasta[1], M G Bisogni[2], A Del Guerra[2], S Marcatili[2], P Barrillon[3], S Bondil-Blin[3], C de la Taille[3] and C Piemonte[4].

[1]Instituto de Física Corpuscular (IFIC-CSIC/UVEG), Valencia, Spain.
[2]University of Pisa and INFN, Pisa, Italy.
[3]Laboratoire de l'Accélérateur Linéaire, Orsay, France.
[4]Center for Scientific and Technological Research (FBK-irst), Trento, Italy.

E-mail: gabriela.llosa@ific.uv.es

Abstract. The characterization of a PET detector head based on continuous LYSO crystals and silicon photomultiplier (SiPM) arrays as photodetectors has been carried out, for its use in the development of a small animal PET prototype. The detector heads are composed of a continuous crystal and a SiPM matrix with 64 pixels in a common substrate, fabricated specifically for this project. Crystals with three different types of painting have been tested: white, black, and black on the sides but white on the back of the crystal. The best energy resolution, obtained with the white crystal, is 16% FWHM. The detector response is linear up to 1275 keV. The uniformity of the detector channels, including electronics and crystal variations, is within 5%. Tests with different position determination algorithms have been carried out with the three crystals. The spatial resolution obtained with the center of gravity algorithm is 0.9 mm FWHM for the three crystals. As expected, the use of this algorithm results in a displacement of the reconstructed position towards the center of the crystal, more pronounced in the case of the white crystal. A maximum likelihood algorithm has been tested that can reconstruct correctly the interaction position of the photons also in the case of the white crystal.

Keywords: small animal PET, continuous crystals, silicon photomultipliers, Geiger APD.

1. Introduction

Multicell Geiger-mode avalanche photodiodes, also known as silicon photomultipliers (SiPMs) (Golovin & Saveliev 2004, Renker 2006), are employed in different fields in physics and their development is still ongoing. Their characteristics, among which are high gain, fast timing properties, insensitivity to magnetic fields, and compactness, make them interesting candidates to replace photomultiplier tubes (PMTs) in numerous applications, including medical imaging.

The fabrication of 2D arrays (matrices) that provide position information has favoured their use in medical imaging applications, in particular in Positron Emission Tomography (PET). In this field, solid state photodetectors offer the possibility to implement or improve some novel techniques (Lewellen 2008) such as depth of interaction determination methods or the combination of PET and MR imaging technologies (McElroy et al. 2007, Spanoudaki et al. 2008, España et al. 2010) among others. The fast response of SiPMs makes them also good candidates for time-of-flight (TOF) PET applications (Vinke et al. 2009).

Several groups are studying the performance of PET detector heads with SiPMs in different detector head configurations, both with continuous and pixellated crystals (Schaart et al. 2009, Kolb et al. 2010). The use of continuous crystals results in a higher efficiency than pixellated crystals at a lower cost. Finely segmented photodetectors (solid state photodetectors or multi-anode PMTs) together with position estimation methods based on maximum likelihood algorithms or artificial neural networks, can provide high spatial resolution (Joung et al. 2002, Bruyndonckx et al. 2006, Bruyndonckx et al. 2008, Pani et al. 2008).

In 2005, the University of Pisa and INFN Pisa proposed the development of a small animal PET detector based on continuous crystals and arrays of SiPMs (Moehrs et al. 2006). The proposed system consists of two or four rotating detector heads, each one composed of three detector layers. The layers are made of a continuous LSO crystal coupled to a SiPM matrix structure. With this aim, the Center for Scientific and Technological Research (FBK-irst) has developed monolithic SiPM matrices, that will be employed in the construction of the PET scanner. Monolithic matrices have the advantage that the signal is routed from each pixel to the side of the detector by means of readout lines instead of wire-bonds that require more space, and thus the dead area between the pixels can be minimized. In addition, the doping profiles of all the pixels in the matrix are very similar, and therefore the characteristics of the pixels are very uniform.

After a development period (Piemonte 2006, Piemonte 2007, Llosá 2009), matrices with 64 pixels have been fabricated, that will be employed in the construction of a PET detector. The first test detector heads have been constructed, consisting of a continuous LYSO crystal coupled to a SiPM matrix. The characterization of the detector heads has been carried out in collaboration with IFIC, Valencia.

The detector heads tested have been assembled employing continuous crystals with three types of painting. The uniformity of the SiPM matrix has also been evaluated using a pixellated crystal array. The detectors have been characterized in terms of energy and timing resolution. Position determination studies have also been carried out with center of gravity (COG) and maximum likelihood (ML) methods.

2. Materials and methods

2.1. Detector heads

The detector heads tested are composed of a continuous LYSO crystal coupled to a 64-pixel SiPM matrix. Three crystals with different types of painting have been tested, and a pixellated crystal array has also been employed to evaluate the matrix uniformity.

2.1.1. SiPM matrices The matrices are composed of 64 (8x8) SiPM pixels with n-on-p structure in a common substrate (figure 1). The active area of the matrix has 12 mm×12 mm size, and the pixel pitch is 1.5 mm×1.5 mm.

Matrices with three different layouts have been fabricated, with the readout pads on two sides, or on one side. In all cases, the eight pixels in each row are attached

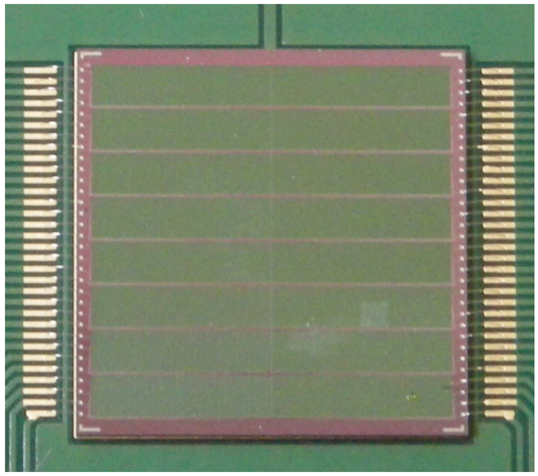

Figure 1. SiPM matrix composed of 64 pixels in a common substrate and readout pads in two opposite sides.

to one another, leaving no physical space between them, but they are electrically independent. Below each row there is a space for the readout lines to reach the sides of the detector.

The matrices with the readout on one side allow to tile several devices with a higher packing fraction. On the other hand, the gap between the pixel rows must be larger and this results in a smaller pixel size. The pixel size is 1.5 mm$\times$1.3 mm or 1.5 mm$\times$1.2 mm in the types with readout on one side, and 1.5 mm$\times$1.4 mm in the type with readout on two opposite sides.

The matrices employed in these tests have readout on two sides, with 32 channels on each side. Each pixel has 840 microcells of 50 μm$\times$50 μm size. The matrix is glued and wire-bonded to a custom-made printed circuit board (PCB) that gives support and bias. A common bias voltage is applied to all pixels in the matrix, through the backplane of the device. The PCB is directly connected to the readout electronics board.

Two matrices have been tested. One of the devices is covered with glue to protect the device and the wirebonds, facilitating the coupling of the crystal and avoiding to damage the sensor. The second one has no glue and the crystals are coupled directly to it without any optical grease. The use of glue results in a slight loss of photon detection efficiency that has been compensated by increasing the bias voltage of the device.

The breakdown voltage is around 30 V in both cases. The device covered with glue is operated at 4.5 V above the breakdown point (overvoltage), and the current is is 150 μA. The device without glue is operated at 4 V overvoltage, and the current is 250 μA. The high current is due to the fact that in the processes of coupling and decoupling the crystals, some pixels have been slightly scratched. Similar results have been obtained with the two matrices tested. The most representative values are shown in this work.

2.1.2. LYSO crystals Tests have been carried out with LYSO crystals from Hilger Crystals‡. Two kinds of crystals have been employed in the tests reported here: a pixellated crystal array, and three continuous crystals with different types of painting (figure 2). The crystal array consists of 64 pixels of 1.4 mm×1.4 mm×10 mm size, separated by 100 μm of white epoxy resin. The array has been employed to test the uniformity among channels. The continuous crystals are 12 mm×12 mm×5 mm size. The so called *white slab*, is painted in white in 5 faces. The *black slab* is painted in black in 5 faces. The *black and white (BW) slab* is painted in white on the back (the 12 mm×12 mm face opposite to the face that is coupled to the matrix) and in black on the sides. A dedicated holder has been fabricated for a precise positioning of the crystals.

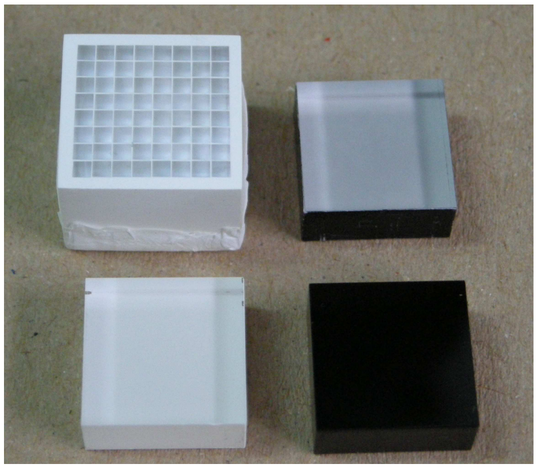

Figure 2. Crystals employed for the tests. Top left: crystal array. Bottom left: white slab. Bottom right: black slab. Top right: black and white slab.

2.2. Readout electronics

The 64-channel ASIC MAROC2 (Barrillon 2007) is employed for the readout of the SiPM matrix. This ASIC has been designed for the readout of multi-anode photomultiplier tubes (Hamamatsu H7546) employed in the Roman Pots of the ATLAS luminometer (ATLAS Collaboration. 2007). The ASIC has not been optimized for PET applications, and its performance could be improved in some aspects. Nevertheless, it has been successfully employed for the tests carried out with SiPMs.

Each channel hosts a preamplifier with a 6-bit adjustable gain stage. A slow shaper with variable shaping time provides the shaped signal, the amplitude of which is proportional to the input charge. The shaping time was set to the longest possible (about 120 ns) to integrate the LYSO signals. The channel trigger is generated by a fast shaper with 15 ns shaping time followed by a level discriminator common to all channels, and controlled by a 12-bit DAC.

The packaged ASIC is soldered on a test board, and driven by an FPGA ALTERA Cyclone§ that controls the data acquisition. A 12-bit ADC located on the test board

‡ www.hilger-crystals.co.uk
§ www.altera.com

digitizes the signals coming from the slow shapers, which are multiplexed in a single analog charge output.

The trigger signal of the detector head is generated by the FGPA as the OR signal of the 64 trigger outputs of the ASIC channels. The trigger is employed to generate a $HOLD$ signal in an external NIM gate generator, which is sent back to the board to sample the shaped signal at its maximum.

In the cases in which we operate the detector head in coincidence with another detector, the signal generated by the second detector is sent to the FPGA on the board after being discriminated. The AND of the trigger signal of the ASIC and the signal of the second detector gives the coincidence trigger. The operation of the board in coincidence with a second detector, that varies depending on the type of study that is being carried out, is represented in figure 3. An oscilloscope is employed to monitor the signals and to acquire the data in the case of the timing measurements.

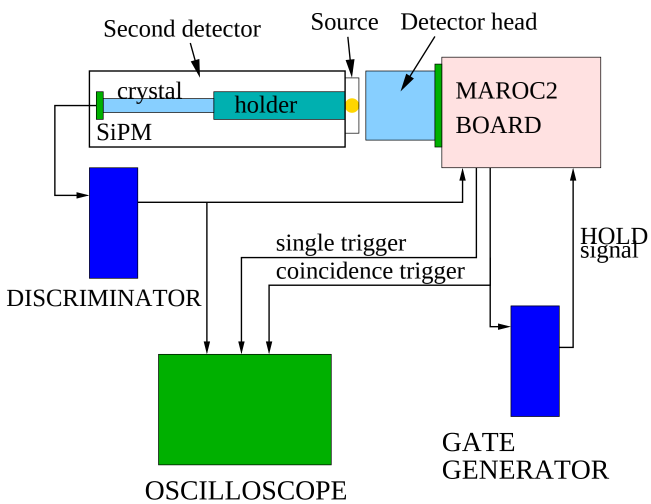

Figure 3. Schematic representation of the setup.

The width of the coincidence signal is given by the overlap of the single triggers of the two devices. The width of the ASIC trigger has been adjusted to the minimum possible, about 130 ns. The coincidence gate width ranges from 25 ns to about 200 ns. The wide window results in the acquisition of random events that generate noise in the data acquired.

The board is controlled by a computer through the USB port, employing a dedicated software developed for the ASIC test and data acquisition.

Tests have been carried out to determine the ASIC response, employing a pulse generator. A calibration pulse is sent to the calibration input, through a 47 nF capacitor. Figure 4(a) shows the ASIC response to an injected calibration pulse as a function of the injected charge for five channels. The ASIC has a linear response from 10 pC to about 80 pC, with a uniformity in the channel response of about 1%, and then it begins to deviate from linearity until it reaches complete saturation. The typical signals coming from the SiPM matrix are in the linear region.

The timing response of the ASIC for one channel has been evaluated with two different pulse generators, measuring the time difference from the calibration pulse to the generated trigger. The contribution of the electronics has been estimated by determining the time difference between the calibration pulse and the synchronized output of the pulse generator, being different in the two cases. Subtracting the contribution of the electronics, the timing jitter of the ASIC is around 330 ps FWHM in both cases. Figure 4(b) shows the measured timing distribution, including the contribution of the electronics that in this case is about 140 ps FWHM.

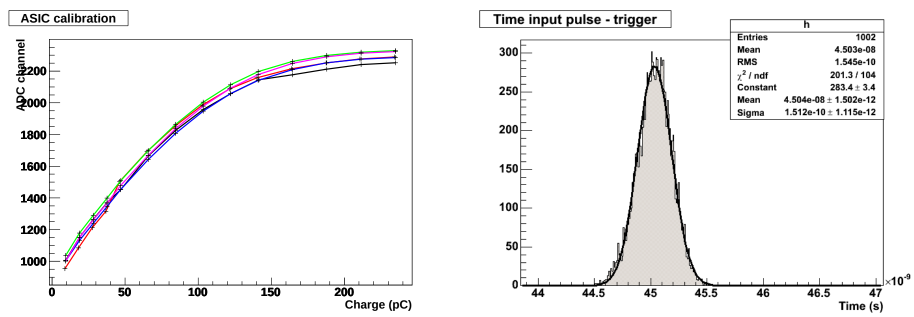

(a) ASIC response

(b) Timing distribution

Figure 4. ASIC studies. (a) Response to the input pulse for five channels. (b) Timing response.

3. Characterization studies

The response of the detector head with different crystals has been characterized. The detector uniformity, linearity, energy and timing resolution have been evaluated. Additionally, position determination studies have also been carried out.

3.1. Response uniformity

The uniformity of the 64 channels has been evaluated employing the crystal array. The crystal array is coupled one-to-one to the pixels in the matrix, so that each SiPM pixel detects the light coming from one crystal.

With the crystal array and the matrix biased at 4.5 volts overvoltage, the amount of light per pixel is much higher than in the case of continuous crystals, and it saturates the ASIC preamplifier. As a consequence, the system can not be operated at the same bias voltage applied in the tests with continuous crystals. In order to have signals in the individual pixels in the same range as the ones obtained with continuous crystals, so as to make this study at a similar signal level, the voltage has been lowered to 2V overvoltage. Only the matrix protected with glue has been employed for this test, given that it is not possible to couple the crystal array to the other matrix without touching the wirebonds.

A ^{22}Na energy spectrum is acquired for each channel, and the photopeak is fitted with a Gaussian function, to compare the photopeak position of all channels.

Table 1. Sources employed for the detector calibration.

Isotope	Energy (keV)
^{57}Co	122
^{133}Ba	356
^{22}Na	511
	1275
^{137}Cs	662
^{54}Mn	835

3.2. Energy resolution

SiPMs are known to saturate for a high number of photons arriving to the detector with respect to the number of microcells, producing a deviation from linearity in the detector response that can alter the appropriate determination of the energy resolution (Renker 2006). It is thus necessary to correct for this deviation, or to check the linearity of the device in order to ensure that the results are not affected by this effect. In our case, the white crystal is the one that gives a higher amount of light per pixel, and hence it has higher probability to saturate the photodetector. For this reason, this crystal is employed for the calibration tests.

Data have been taken with different sources to test the response up to 1275 keV. The sources employed are listed in table 1. When employing continuous crystals, the light generated in the crystal from each event is detected by several pixels in the matrix, and to determine the energy deposited in the interaction, the ADC values of all the pixels that trigger are summed for each event.

The energy resolution has been evaluated for the three continuous crystals at 511 keV employing a ^{22}Na source.

3.3. Timing resolution

The coincidence timing resolution has been evaluated for the three continuous crystals. Tests have been carried out setting the detector head in coincidence with a 5.5 mm×5.5 mm×5 mm BaF_2 crystal coupled to a PMT Hamamatsu H5783‖.

The time difference between the trigger signal provided by the MAROC2 board, and the signal of the second detector has been measured employing an oscilloscope LeCroy *wavepro* 940¶. The BaF_2 signal triggers the acquisition, and the time difference is histogrammed if the MAROC2 signal arrives within a 800 ns time window.

Both the discriminator in the MAROC2 ASIC and the one employed for the second detector are level discriminators, and only one threshold value can be set. If the threshold is set low to improve the timing performance (Post & Schiff 1950) the measurements are affected by time-walk due to the differences in the amplitude of the signals measured.

3.4. Position determination

Position determination studies have been carried out with the three continuous crystals. In order to restrict the interaction position of the photons to the one desired,

‖ www.hamamatsu.com
¶ www.lecroy.com

the photons of a ^{22}Na source are electronically collimated by operating the detector head in coincidence with a second detector, as described in section 2 (see figure 3). In this case, the second detector consists of a 1 mm×1 mm×10 mm LYSO crystal coupled to a 1 mm×1 mm SiPM. The radioactive source is attached to the second detector at 3 cm distance by means of a source holder, and set as close as possible to the detector head (about 0.5 mm from the crystal surface). The second detector with the source attached is moved with three motorized stages controlled from the computer.

For each of the three crystals studied here, a scan of the detector area is carried out taking data at 2 mm steps. In addition, in order to improve the determination of the light response function (LRF) in the position determination studies, a scan with 1 mm steps is also performed with the BW slab.

The source employed for this test is a point-like ^{22}Na source from Isotrak HTSL[+] with a nominal diameter of 1 mm. It has a low activity (about 34 kBq), which yields a low coincidence rate. In addition, the large coincidence window results in the acquisition of a non-negligible amount of background events, mainly due to accidental coincidences and intrinsic LYSO activity, due to the presence of radioactive isotope ^{136}Lu in the crystal.

Two methods have been tested for the determination of the interaction position in the continuous crystals. In the Anger or COG method (Anger 1958), the interaction position is determined by calculating the weighted mean of the event. The reconstructed position is given by the average of the positions of the n pixels that trigger (x_i, y_i), weighted with the energy recorded for each pixel, or a proportional quantity such as the measured ADC value, ADC_i.

$$x = \frac{\sum_{i=1}^{n} x_i ADC_i}{\sum_{i=1}^{n} ADC_i}, y = \frac{\sum_{i=1}^{n} y_i ADC_i}{\sum_{i=1}^{n} ADC_i}, \tag{1}$$

The COG method is known to distort the reconstructed positions, that are compressed towards the center of the crystal, in particular with white crystals in which the light reflects at the sides. With the aim of improving the position determination, a ML method has also been tested (Gray & Macovski 1976, Fessler et al. 1991). The proposed method estimates the location of the interaction point given the response of the PMTs in an Anger scintillator camera. In this method, the response of the PMTs is based on the solid angle subtended by the PMT from the interaction point. In our case, instead of employing the solid angle, we have modelled the response of the SiPM pixels measuring the LRF of each pixel as a function of the interaction position of the photons.

The reconstructed interaction position is the one that maximizes the following expression:

$$P(x, y) = \sum_{i=1}^{n} ADC_i \times LRF_i(x, y) - LRF_i(x, y); \tag{2}$$

where $LRF_i(x, y)$ is the LRF of the i^{th} SiPM element, i.e, the amount of light detected by the SiPM for the photons interacting in a given position, ADC_i is the measured ADC value for pixel i, and n is the number of pixel elements that trigger in each event.

[+] www.hightechsource.co.uk

4. Results and Discussion

4.1. Pixel response uniformity

The crystal array has been coupled to the matrix, and data have been taken with a ^{22}Na source. An energy spectrum has been obtained for each channel, and the photopeak position has been determined by fitting a Gaussian function. The mean value of the photopeak position for each channel, as a function of the pixel location, is shown in figure 5(a). Figure 5(b) shows the distribution of the peak positions of the 64 channels, fitted with a Gaussian function. The distribution of the peak positions, which includes variations of the electronics and crystals, has a standard deviation of 5% proving the good uniformity of the matrix.

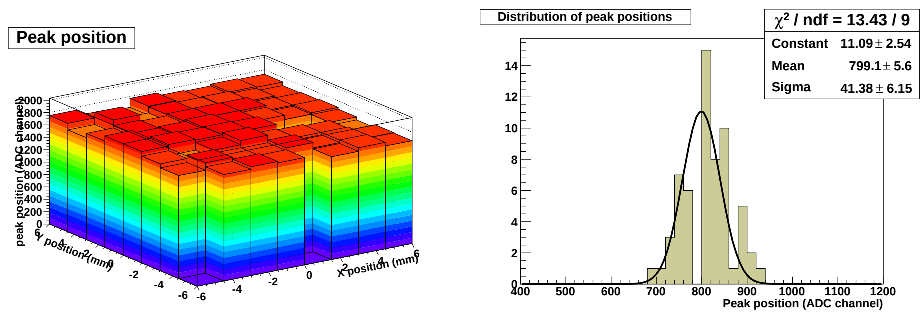

(a) Peak positions (b) Peak position distribution

Figure 5. Pixel response uniformity. (a) 2D plot of the ^{22}Na photopeak position for all pixels in the matrix. (b) Distribution of the mean values of the fitted photopeak positions. The variation is within 5%.

4.2. Energy resolution

In order to ensure the linear response of the detector, the white crystal has been coupled to the matrix, and data have been taken with sources of different energies (table 1). The photopeak position in each case has been obtained by fitting a Gaussian function, and the mean value is plotted versus the source energy. The result, shown in figure 6, ensures that the device does not saturate, and thus there is no need to correct the data for deviations from linearity to determine the energy resolution.

The energy resolution at 511 keV is evaluated for each crystal, taking data with a ^{22}Na source. Table 2 shows the results for the three crystals. Figure 7 shows the calibrated ^{22}Na energy spectrum obtained with the white crystal. Correcting for the variations among channels, described in the previous sections, has shown no significant improvement in the spatial resolution, and therefore these corrections are not applied here. The white crystal has a better energy resolution than the black and BW crystals, given that the reflection of the light on the sides and the back of the crystal results in a larger amount of light reaching the photodetector.

4.3. Timing resolution

The timing resolution with the three continuous crystals has been measured with the setup described in section 2, in coincidence with a BaF_2 crystal coupled to a PMT. The

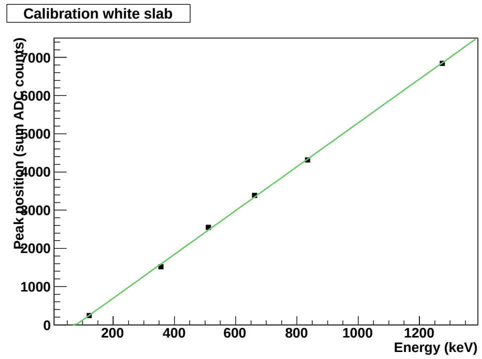

Figure 6. Response of the detector to different energies, showing the linear behaviour up to 1275 keV.

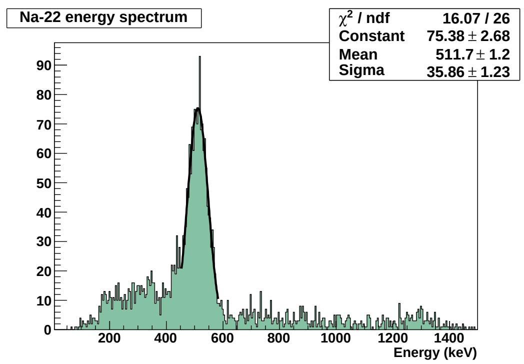

Figure 7. Calibrated ^{22}Na energy spectrum. The energy resolution is 16% FWHM.

Table 2. Energy resolution measured for the three crystals.

Crystal	Energy resolution (FWHM)
white	16%
black and white	30%
black	26%

timing resolution has been measured by histogramming the time difference between the trigger signals of the two devices with an oscilloscope. The data acquisition is triggered by the PMT signal in the oscilloscope, with a fixed threshold set at 25% of the signal. The MAROC2 threshold is varied to obtain the best possible timing resolution. An example of the resulting timing distribution obtained is shown in figure 8. At low threshold, the peak is narrower, but it has a tail due to the time-walk effect. As the threshold is increased, the tail is reduced, but the timing resolution degrades.

The results obtained with the different crystals are summarized in table 3. The use of continuous crystals results in a relatively low amount of light per pixel, which gives poor timing performance. For the black and BW crystals, which have a lower

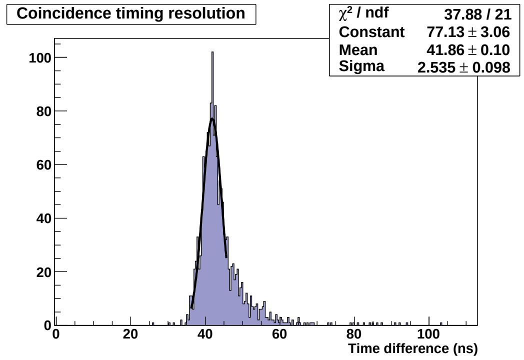

Figure 8. Coincidence timing resolution of the detector head with the white crystal and a BaF_2 crystal coupled to a PMT.

Table 3. Coincidence timing resolution between the detector head and the BaF_2 crystal coupled to a PMT.

Crystal	Timing resolution (ns FWHM)
white	6.04
black and white	8.70
black	6.79

amount of light per pixel, the performance is worse than for the white crystal.

The ASIC has a fast intrinsic response, but it is not optimized for timing measurements with continuous crystals. Possible improvements are being considered to enhance the timing performance. One option is to implement a double threshold system that allows to trigger at low thresholds, while selecting only the photopeak signals desired in PET applications. Another possibility that will be considered is to employ the signal given by the sum of the signals of all pixels to generate the trigger.

4.4. Position determination

Position determination studies have been carried out as described in section 3.4. Scans across the crystal surface at 2 mm steps have been performed with the three continuous crystals. In addition, a scan at 1 mm steps has also been carried out for the BW slab. Two methods have been tested to determine the interaction position, the well known COG, and a ML method.

4.4.1. Center of gravity The scan data taken for the three crystals have been reconstructed with the COG algorithm (equation 1). Figure 9(a) shows the 2D distribution of the reconstructed positions at a given interaction position at about the center of the BW crystal, for 1000 events. For the three crystals, the spatial resolution calculated by fitting a Gaussian function to a profile through the maximum of the peak is approximately 0.9 mm FWHM. Figure 9(b) shows the fitted X profile of figure 9(a). A value of 0.85 mm FWHM is obtained. The profiles can be more accurately fitted with a Lorentzian function, which represents better the shape of the reconstructed position distribution,

$$L(x) = \frac{1}{\pi} \frac{\frac{1}{2}\Gamma}{(x - x_0)^2 + (\frac{1}{2}\Gamma)^2}, \tag{3}$$

where x_0 is the mean value, and Γ is the FWHM of the distribution. The resolution resulting from the fit of the Lorentzian function is 0.62 mm FWHM. These values are obtained without deconvolving the contribution of the source size.

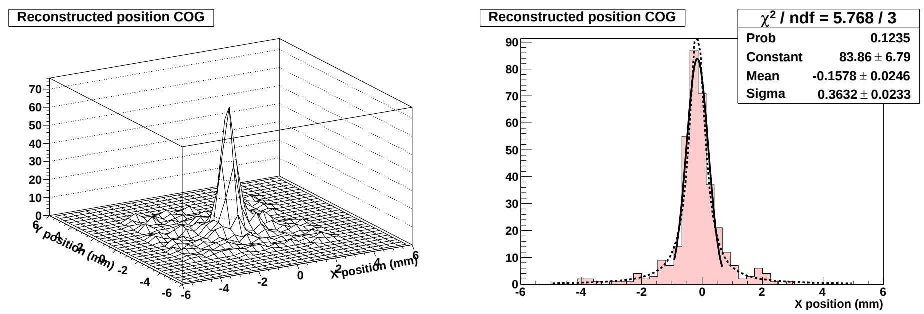

(a) 2D distribution (b) Profile through maximum

Figure 9. Distribution of reconstructed interaction positions with the COG method for a given interaction position close to the center of the crystal. (a) 2D distribution. (b) Fit of a profile through the maximum of the distribution. The spatial resolution is 0.85 mm FWHM fitting the peak with a Gaussian function (solid line) and 0.62 mm FWHM fitting it with a Lorentzian function (dashed line).

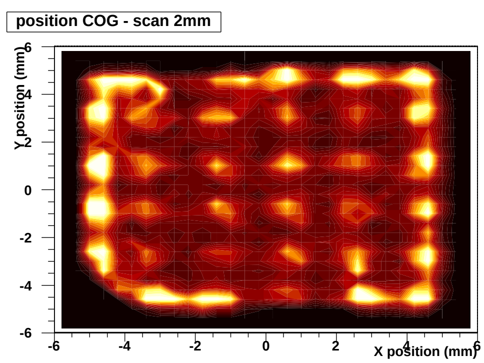

Figure 10. Reconstructed positions with the COG algorithm for the 2 mm scan with the black crystal.

Figure 10 shows all the reconstructed positions for the whole crystal surface obtained with the black slab. Figures 11(a) to 11(c) show the mean values of the peak position of the reconstructed data in the X and Y directions, for the black, BW and white crystals respectively. The crosses represent the nominal interaction positions (which are not exactly the real interaction positions in the crystal, since the alignment between the two detectors is not perfect), and the squares are the corresponding reconstructed positions. For the black crystal, the reconstructed positions correspond to the nominal positions in the center of the crystal, but not those close to the edges of the crystal. In the case of the white crystal, all the reconstructed positions are compressed towards the center of the crystal.

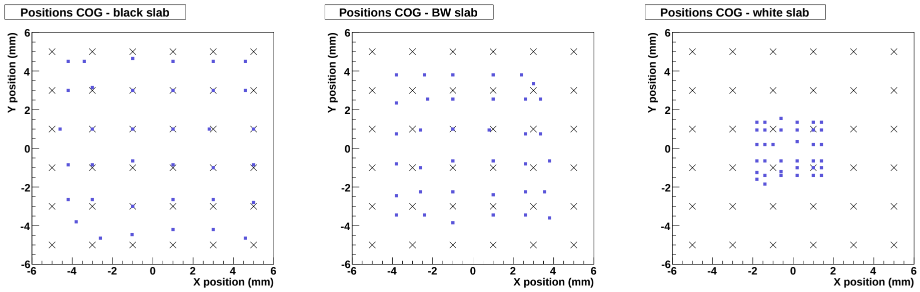

(a) black slab (b) BW slab (c) white slab

Figure 11. Maximum of the reconstructed position (squares) and nominal interaction position (crosses) of the 2 mm scan for the three crystals with the COG algorithm. With this method, the reconstructed positions are compressed towards the center of the crystal. This effect is more pronounced in the case of the white crystal due to the reflections of the light on the sides.

As expected, the COG method fails to identify correctly the interaction points as they approach the edges of the detector. This effect is more pronounced in the case of the white crystal, since the light reflections contribute to distort the reconstructed position.

4.4.2. Maximum likelihood A ML position determination method has been tested with the aim of improving the position reconstruction at the edges of the crystal, in particular in the case of the white crystal.

The LRFs of the pixels are determined employing the data taken at steps of 2 mm for the three crystals, and 1 mm for the BW crystal. The LRF is obtained by representing the average ADC value measured for a given pixel in each of the scanned positions. The measured data are interpolated to have a finer sampling of the LRF.

The LRF of one of the central pixels, measured at 1 mm steps with the BW slab is shown in figure 12. Figure 12(a) shows the average ADC values obtained at the scanned positions, and figure 12(b) shows the interpolated LRF. Even at 1 mm steps, which are smaller than the pitch of the matrix, the sampling is not uniform, and a finer sampling (0.5 mm steps) would provide a better representation of the pixel response.

The measured LRFs are employed for the determination of the interaction position with equation 2. Data taken in test positions are reconstructed with the same accuracy as the data taken in the scanned positions. This method provides a sharp peak at the reconstructed position, and a background of mispositioned events, corresponding mostly to noise events (figure 13(a)). Figure 13(b) shows the reconstructed positions for the 2 mm scan. If the data taken at 1 mm steps are employed for the position determination, this method is able to separate positions at 1 mm distance.

Employing this method, the reconstructed positions correspond to the real positions also at the edges of the detector, even in the case of the white crystal, up to 1 mm from the sides of the crystal.

This method improves the position determination at the edges of the crystal even with white crystals, but it requires longer reconstruction times than the COG method.

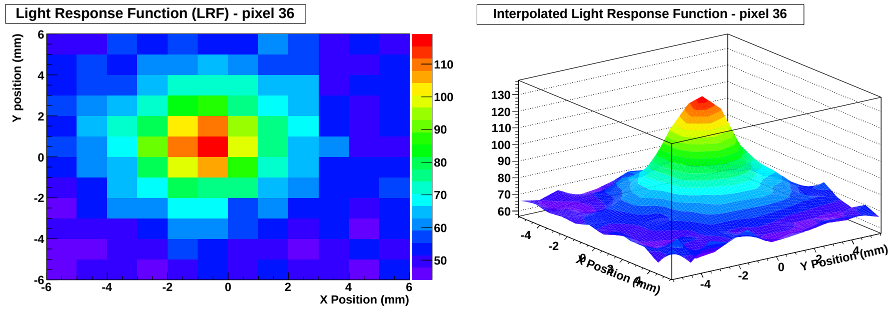

(a) LRF

(b) Interpolated LRF

Figure 12. LRF of one of the central pixels of the matrix measured at 1 mm steps with the BW crystal. (a) Average ADC value measured at each position. (b) Interpolated function represented in 2D.

Studies are being carried out to improve the method and increase the reconstruction speed by modelling the LRF. In addition, other position reconstruction methods are being tested (Moehrs et al. 2006).

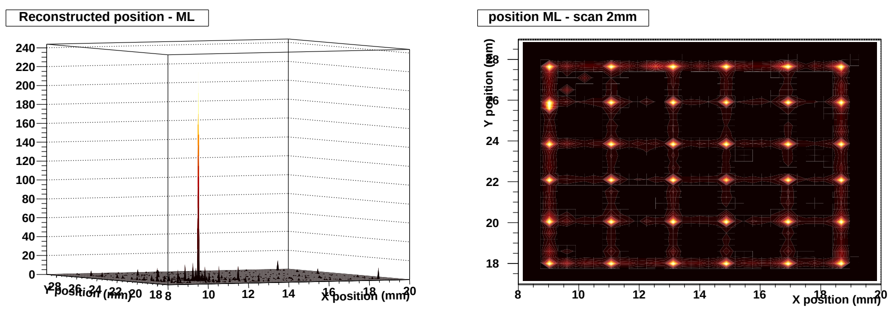

(a) Reconstructed position

(b) All scanned positions

Figure 13. Interaction positions reconstructed with the ML method. (a) Reconstructed distribution in a given position. (b) Reconstructed positions for the 2D scan with the black crystal.

5. Conclusions and future work

The performance characterization of a detector head with continuous crystals and monolithic 64-pixel SiPM matrices, for its use in the construction of a small animal PET system, has been completed. The MAROC2 ASIC has been employed as readout electronics. The results presented assess the correct functioning of the photodetector and the electronics, and the good performance of the detector head.

Continuous crystals with different types of painting (white, black and white, and black), have been coupled to the matrix and characterized. A crystal array has been employed to test the uniformity of the detector, that is within 5%. A very good energy resolution, around 16% FWHM at 511 keV, has been obtained with the white crystal. As expected, the energy resolution is degraded for the BW and the black slabs, since the light that is emitted towards the sides of the crystal is absorbed, and it does not reach the photodetector. The linearity of the detector has also been tested with the white crystal up to 1275 keV, showing a linear response in the whole range.

The timing resolution obtained is around 6-8 ns FWHM, for the different crystals tested. The low amount of light per SiPM pixel in the case of continuous crystals results in a relatively poor timing resolution with the setup employed for these tests. The possibility of improving the timing performance by using a double threshold system to be able to trigger at the single photoelectron level is being studied. Employing the sum of the signals of all pixel elements for triggering is also being considered.

An excellent spatial resolution, better than 0.9 mm FWHM with the COG algorithm, has been obtained. As expected, the COG method fails to reconstruct the real interaction position close to the edges with the black crystal, and in the whole surface for the white crystal. This effect can be corrected with a good position calibration, but is subject to errors, in particular with the white crystal in which the reconstructed positions are very close to one another. A ML method has been successfully applied that improves the position determination also in the case of white crystals, providing the correct position in the whole surface with the three crystals.

The white crystal offers a much better performance in terms of energy and timing resolution. If the interaction positions can be properly and efficiently reconstructed, this makes it the crystal of choice for our imaging system.

In order to study the performance of the detector head in an imaging system, a rotating setup with two detector heads in coincidence is being assembled, which will allow us to acquire tomographic data. We will also continue to improve the detector performance, mainly enhancing the timing resolution and shortening the coincidence window in order to reduce the noise. The position determination studies will continue for a further improvement of the method.

Acknowledgments

This work is partially supported by the European Commission's Seventh Framework Programme through a Marie Curie Reintegration Grant.

References

Anger H O, 1958. Scintillation Camera. *Rev. Sci. Instrum.* **29**, 27–34.

Barrillon P et al, 2007. MAROC: Multi-anode readout chip. *2007 IEEE NSS MIC Conf. Rec. CD-ROM* .

Bruyndonckx P, Lemaitre C, van der Laan D, Maas M, Schaart D, Wang Y, Li Z, Krieguer M & Tavernier S, 2008. Evaluation of machine learning algorithms for localization of photons in undivided scintillator blocks for PET detectors. *IEEE Transactions on Nuclear Science* **55**(3), 918–924.

Bruyndonckx P, Leonard S, Lemaitre C, Tavernier S & Wu Y, 2006. Performance study of a PET detector module based on a continuous scintillator. *IEEE Transactions on Nuclear Science* **53**(5), 2536–2542.

Atlas Collaboration, 2007. ATLAS Forward Detectors for Measurement of Elastic Scattering and Luminosity Determination. *Technical Design Report, CERN/LHCC/2007-004* .

España S, Fraile L M, Herraiz, J L, Udias J M, Desco M & Vaquero J J, 2006. Performance evaluation of SiPM photodetectors for PET imaging in the presence of magnetic fields. *Nuclear Instruments and Methods in Physics Research Section A* **613**(I 2), 308–316.

Fessler J, Rogers W & Clinthorne N H, 1991. Robust Maximum-Likelihood Position Estimation in Scintillation Cameras. *1991 IEEE NSS MIC Conf. Record.* **1-3**, 1851–1855.

Golovin V & Saveliev V, 2004. Novel type of avalanche photodetector with Geiger mode operation. *Nuclear Instruments and Methods in Physics Research Section A* **518**, 560–564.

Gray M R & Macovski A, 1076. Maximum a posteriori estimation of position in scintillation cameras. *IEEE Transactions on Nuclear Science* **23**(I 1), 849–852.

Joung J, Miyaoka R & Lewellen T, 2002. cMiCE: a high resolution animal PET using continuous LSO with statistics based positioning scheme. *Nucl. Instrum. Meth. A* **489**, 584–598.

Kolb A, Lorenz E, Judenhofer M, Renker D, Lankes L & Pichler B, 2010. Evaluation of Geiger-mode APDs for PET block detector designs. *Physics in Medicine and Biology* **55**(I 7), 1815–1832.

Lewellen T. 2008. Recent developments in PET detector technology. *Physics in Medicine and Biology* **53**, 287–317.

Llosá G et al. 2009. Energy, timing and position resolution studies with 16-pixel SiPM matrices for PET applications. *IEEE Transactions on Nuclear Science* **56**(I 5), 2586–2593.

McElroy D, Saveliev V, Reznik A & Rowlands J.2007. Evaluation of silicon photomultipliers: A promising new detector for MR compatible PET. *Nuclear Instruments and Methods in Physics Research Section A* **571**, 106–109.

Moehrs S, Del Guerra A, Herbert D & Mandelkern M. 2006. A detector Head design for small animal PET with silicon photomultipliers (SiPM). *Physics in Medicine and Biology* **51**, 1113–1127.

Pani R, Vittorini F & Pellegrini R. et al. 2008. High spatial and energy resolution gamma imaging based on LaBr3(Ce) continuous crystals. *2008 IEEE NSS MIC conference Record* pp. 1763–1767.

Piemonte C. 2006. A new Silicon Photomultiplier structure for blue light detection. *Nuclear Instruments and Methods in Physics Research Section A* **568**(I 1), 224–232.

Piemonte C et al. 2007. Recent Developments on Silicon Photomultipliers produced at FBK-irst. *2007 IEEE NSS MIC Conf. Record. CD-ROM.* (N41-2.).

Post R & Schiff L.1950. Statistical Limitations on the Resolving Time of a Scintillation Counter. *Physical Review.* **80**(I 6), 1113–1113.

Renker D. 2006. Geiger-mode avalanche photodiodes, history, properties and problems. *Nuclear Instruments and Methods in Physics Research Section A* **567**(1), 48–56.

Schaart D R, van Dam H T, Seifert S, Vinke R, Dendooven P, Löhner H & Beekman F. 2009. A novel, SiPM-array-based, monolithic scintillator detector for PET. *Physics in Medicine and Biology* **54**, 3501–3512.

Spanoudaki V, Mann A, Hohberg M, Konorov I, Paul S & Ziegler S A. 2008. Silicon Photomultiplier based novel detector concept for combined PET/MR. *Journal of Nuclear Medicine* **49**, 65.

Vinke R, Löhner H, Schaart D R, van Dam H, Seifert S, Beekman F & Dendooven P. 2009. Optimizing the timing resolution of SiPM sensors for use in TOF-PET detectors. *Nuclear Instruments and Methods in Physics Research Section A* **610**, 188–191.